Flight Path Control for a Multi-body HALE Aircraft

Alexander Köthe and Robert Luckner

1 Introduction

High Altitude Long Endurance (HALE) aircraft have become an interesting alternative for satellites, e.g. for communication and surveillance tasks, since they offer more flexibility in operation. Due to their lightweight construction, their high-aspect-ratio and the use of solar panels, they can be operated in the stratosphere for up to 336 h (cf. QinetiQ Zephyr [9]). In contrast to satellites, HALE aircraft are not bound to a specific trajectory. They can be operated in a specific region for a certain amount of time. When a mission is completed, they can be recovered, relocated and used for another mission. Current HALE aircraft have large wing spans that can lead to large deformation with structural geometrical nonlinearities. On the flight to the mission altitude, HALE aircraft have to pass the troposphere, in which most of the weather events (gusts, turbulences) occur. Gusts may cause high aerodynamic loads leading to high wing bending moments that influence the fatigue strength of the aircraft. Additionally, non-uniform gust excitations of the highly flexible vehicle may result in larger deformations than caused by uniform ones [17]. A new alternative to one-wing HALE aircraft are Multi-Body Aircraft (MBA) that are investigated at TU Berlin's department of Flight Mechanics, Flight Control and Aeroelasticity. This concept is based on the linkage of several individual rigid-body aircraft to a single HALE aircraft in the mission altitude. A high-aspect-ratio can be accomplished without consideration of structural geometrical nonlinearities. Moreover, each single aircraft can be brought to the stratosphere with a helium balloon or fly on their own up to the mission altitude ensuring low aerodynamic loads and hence bending moments due to atmospheric disturbance in the troposphere. Lastly, the modularity

A. Köthe (✉) · R. Luckner
Technische Universität Berlin, Marchstraße 12, 10587 Berlin, Germany
e-mail: alexander.koethe@campus.tu-berlin.de

R. Luckner
e-mail: robert.luckner@tu-berlin.de

B. Dołęga et al. (eds.), *Advances in Aerospace Guidance, Navigation and Control*, https://doi.org/10.1007/978-3-319-65283-2_23

of a MBA permits exchange and return to ground of a single individual aircraft for repairing purposes without significantly affecting the flight mission.

A flight mechanic design for such a MBA HALE based on the DARPA Vulture program specification [11] was carried out. The objective of the Vulture program is the development of a heavier-than-air aircraft that can be operated with a payload of 1,000 lb (450 kg) over a period of five years. Besides those flight performance specifications, every aircraft has to be designed with a nearly rigid wing that leads to a heavier wing structure with negligible structural modes. For the coupling in the mission altitude each aircraft has to be able to fly individually. Therefore, the aircraft requires an adequate wing to produce sufficient lift, a horizontal and vertical stabilizer for stability, control surfaces (ailerons, elevator and flaps) for lateral and vertical controllability and a flight control system. The result of the design process was a formation with ten coupled aircraft that possesses a total wing span of 215 m with an aspect ratio of 66.8 and a total mass of 4090 kg. Additionally the outer aircraft of the MBA have a dihedral angle of 2.5°. This 80% cranked semi-span dihedral configuration reduces the span width, since the Oswald parameter is positive affected. The MBA HALE is able to fly 365 days in the mission altitude of 20 Km with a payload of 450 kg and a maximum (north or south) latitude of 40°. The detailed properties are given in Table 1. Figure 1 presents a illustration of the designed MBA HALE. As controls, the left and right flaps along the complete half span, an elevator, a rudder and one engine of each aircraft are used. In total the MBA has 50 control inputs.

A previous general concept investigation showed that an optimal linkage of two aircraft can be achieved with a joint that allows a pitch and roll motion between two aircraft and restrict a yaw motion [8]. As a consequence the degrees of freedom are much higher in comparison to a conventional fixed wing aircraft. This has an impact on the flight control system. This paper describes the development of a flight path control law for altitude and heading control. The flight control law is structured into the inner-loops that ensure damping as well as attitude and airspeed control and the outer-loop for altitude and heading control. The flight dynamics of the formation are discussed and the requirements that are derived from the aircraft design mission and the flight mechanical analysis are defined. The control law structure for the

Table 1 Properties of the designed Multi-body High Altitude Long Endurance Aircraft

Coupled aircraft	$i = 10$	Mission altitude	$H = 20$ km
Mission latitude	$Lat \leq 40°$	Complete span width	$b = 215.27$ m
Aspect ratio	$\Lambda = 66.76$	Total mass	$m = 4089.9$ kg
Design speed	$V = 33.15 \frac{\text{m}}{\text{s}}$	Required energy	$E_{\text{req}} = 3.2212$ GJ
Design lift coefficient	$C_L = 1.242$	Zero drag coefficient	$C_{D,0} = 0.0061$
Total payload	$m_{\text{Pay}} = 450$ kg	Required payload power	$P_{\text{req,pay}} = 5$ kW

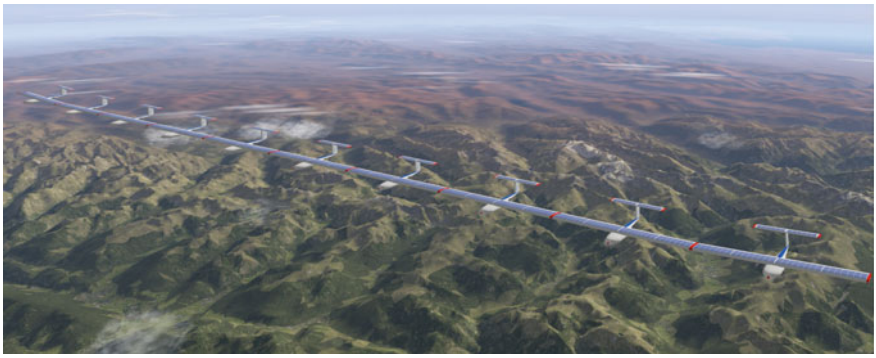

Fig. 1 Illustration of the designed Multi-body High Altitude Long Endurance Aircraft

inner-loop and outer-loop is introduced and the controller gains are determined. The control laws are tested in linear and nonlinear simulations for command following and disturbance rejection.

2 Flight Dynamics of Multi-body Aircraft

The flight dynamic model of the MBA for the flight control design is basesd on the equations of motion and models of external forces and moments (aerodynamics, thrust and weight). The equations of motion for the Multi-Body Aircraft are assembled following Kane's formalism [7] by using the software tool Autolev / Motion Genesis [10]. Aerodynamic forces and moments are modeled by a Vortex-Lattice method. Based on those methods and the design parameter, a nonlinear flight dynamic model is build up in Simulink. This model is linearized and analyzed by numerical perturbation.

2.1 Equations of Motion

The origin of the equations of motion is Kane's dynamical equation,

$$\tilde{\mathbf{F}}_r + \tilde{\mathbf{F}}_r^{\star} = 0 \quad (r = 1, \ldots, p)\,, \tag{1}$$

where $\tilde{\mathbf{F}}_r$ are the generalized active forces, $\tilde{\mathbf{F}}_r^{\star}$ are the generalized inertial forces and p is the number of degrees of freedom of the system in the reference frame. In Eq. 1, the denotation "generalized force" includes inertial and active forces as well as inertial and active moments (translation and rotation) [7]. The generalized inertial force is determined by

$$\tilde{\mathbf{F}}_r^{\star} = -\sum_{j=1}^{l} {}^{N}\mathbf{F}_k^{CG,j} \frac{\partial {}^{N}\mathbf{v}^{CG,j}}{\partial u_r} - \sum_{j=1}^{l} {}^{N}\mathbf{M}_k^{CG,j} \frac{\partial {}^{N}\omega^{B,j}}{\partial u_r}, \tag{2}$$

where ${}^{N}\mathbf{v}^{CG,j}$ is the velocity of the centre of gravity of the jth body in the Newtonian frame, ${}^{N}\omega^{B,j}$ the angular velocity of the body frame against the Newtonian frame of the jth body, u_r the generalized speeds and $\mathbf{F}_k$ and $\mathbf{M}_k$ are the mass force and mass torque of the jth body decomposed as

$${}^{N}\mathbf{F}_k^{CG} = m\left(\frac{d\,{}^{B}\mathbf{v}^{CG}}{dt} + {}^{N}\omega^{B} \times {}^{B}\mathbf{v}^{CG}\right) \quad \text{and} \quad {}^{N}\mathbf{M}_k^{CG} = \mathbf{I}\,{}^{N}\dot{\omega}^{B} + {}^{N}\omega^{B} \times \left(\mathbf{I}\,{}^{N}\omega^{B}\right), \tag{3}$$

and l the number of rigid bodies in the system. The generalized active force is given by

$$\tilde{\mathbf{F}}_r = \sum_{j=1}^{l} {}^{N}\mathbf{F}_A^{CG,j} \frac{\partial {}^{N}\mathbf{v}^{CG,j}}{\partial u_r} + \sum_{j=1}^{l} {}^{N}\mathbf{M}_A^{CG,j} \frac{\partial {}^{N}\omega^{B,j}}{\partial u_r}, \tag{4}$$

where $\mathbf{F}_A$ and $\mathbf{M}_A$ are the active forces and moments acting at or around the center of gravity. Both, velocities and angular velocities in Eqs. 2 and 4 are based on generalized speeds u_r $(r = 1, \ldots, p)$ that are derived from the generalized coordinates q_s $(r = 1, \ldots, n)$, where n is the number of generalized coordinates and p the number of generalized speeds, with

$$u_r = \sum_{s=1}^{n} Y_{rs}\,\dot{q}_s + Z_r \quad (r = 1, \ldots, p) \tag{5}$$

where Y_{rs} and Z_r are functions of the generalized coordinates and time. Equation 5 is called kinematical differential equation [7].

Generalized coordinates and speeds are restricted by constraint equations. Considering a formation of i aircraft, the number of generalized coordinates is determined by

$$n = 6 \times i - M, \tag{6}$$

where M is the number of holonomic constraint equations and every aircraft possesses the position (three Cartesian coordinates) and the orientation against the Newtonian frame (three Euler angles[1]) as generalized coordinates. Holonomic constraints are expressed by the generalized coordinates, while N nonholonomic constraint equations can be expressed as m relationships

[1] Euler angles is the common denotation in flight mechanics. In multi-body dynamics the orientation angles are called Cardan angles.

$$u_r = \sum_{s=1}^{p} A_{rs}\, u_s + B_r \quad \text{with} \quad p = n - m \quad (r = p+1, \ldots, n) \tag{7}$$

where A_{rs} and B_r are functions of the generalized coordinates and time [7]. In case of using Eq. 7, holonomic constraint equations can be formed into nonholonomic constraint equations, but not necessarily vice versa. Hence the number of generalized speeds p is given by

$$p = 6 \times i - M - N. \tag{8}$$

The selected joint of the MBA allows a pitch and roll motion between two neighboring aircraft A and B. The other generalized speeds are restricted with four non-holonomic constraints

$$\begin{matrix} \left({}^N\mathbf{v}^{CAB} - {}^N\mathbf{v}^{CBA}\right)\mathbf{e}_{xg} = 0 & \left({}^N\mathbf{v}^{CAB} - {}^N\mathbf{v}^{CBA}\right)\mathbf{e}_{yg} = 0 \\ \left({}^N\mathbf{v}^{CBA} - {}^N\mathbf{v}^{CAB}\right)\mathbf{e}_{zg} = 0 & \left({}^N\omega^{A} - {}^N\omega^{B}\right)\mathbf{e}_{zg} = 0 \end{matrix}, \tag{9}$$

where CAB is the connection point between both aircraft. The $N = 3$ nonholonomic motion constraints for the body fixed velocities can be further expressed as $M = 3$ holonomic constraint equations. This is no longer applicable for the motion constraints of the rotation. Using the roll rate u_1, pitch rate u_2 and yaw rate u_3 as generalized speeds and the roll angle q_1, pitch angle q_2 and yaw angle q_3 as generalized coordinates, the kinematic differential equations are derived in [14] as

$$\begin{bmatrix} \dot{q}_1 \\ \dot{q}_2 \\ \dot{q}_3 \end{bmatrix} = \begin{bmatrix} 1 & \sin(q_1)\tan(q_2) & \cos(q_1)\tan(q_2) \\ 0 & \cos(q_1) & -\sin(q_2) \\ 0 & \frac{\sin(q_1)}{\cos(q_2)} & \frac{\cos(q_1)}{\cos(q_2)} \end{bmatrix} \begin{bmatrix} u_1 \\ u_2 \\ u_3 \end{bmatrix}. \tag{10}$$

Even if u_3 is equal to zero, pitch and roll rate influence all other generalized speeds due to the nonholonomic motion constraints. Thus, $N = 1$ nonholonomic constraints exist, but no holonomic constraints. As a consequence, every coupled aircraft results in $N = 4$ nonholonomic constraints and $M = 3$ holonomic constraints. Hence a formation with ten coupled aircraft and motion constraints of Eq. 9 has 33 generalized coordinates and 24 generalized speeds. By neglecting the navigation states (Ψ and three Cartesian coordinates), four additional generalized coordinates are removed. The arising equations of motions are highly nonlinear due to the rotational degrees of freedom, but the existing nonlinearities can be described mathematically exact. This is an advantage in comparison to structural nonlinearities that can only be approximated by mathematical models. Linearizing those nonlinear equations leads to a first order differential equation system with 53 states.

2.2 External Active Forces and Moments

The active forces and moments that have to be considered for the equations of motion are: aerodynamic forces (in the aerodynamic reference frame) $\mathbf{R}_A$, thrust (in the body fixed reference frame) $\mathbf{T}$ and weight (in the Newtonian frame) $\mathbf{W}$ of each aircraft as well as aerodynamic moments (in the aerodynamic reference frame) $\mathbf{M}_A$ and thrust moments (in the body fixed reference frame) $\mathbf{M}_T$. For each single aircraft, it is assumed that the thrust acts at the center of gravity. This results in a zero thrust moment. Regarding to Eq. 4, the active force at the jth aircraft in the body fixed reference frame is determined as

$$ {}^{b}\mathbf{F}_A^{CG,j} = \mathbf{T}_{b,a,j}\,\mathbf{R}_{A,a,j} + \mathbf{T}_{b,n,j}\,\mathbf{W}_{n,j} + \mathbf{T}_{b,j}, \tag{11} $$

where $\mathbf{T}_{b,a}$ is the transformation matrix from the aerodynamic reference frame (index a) to the body fixed reference frame (index b) and $\mathbf{T}_{b,n}$ is the transformation matrix from the Newtonian reference frame[2] (index n) to the body fixed reference frame. The active moment of the jth aircraft in the body fixed reference frame for Eq. 4 is computed with

$$ {}^{b}\mathbf{M}_A^{CG,j} = \mathbf{T}_{b,a,j}\,\mathbf{M}_{A,a,j} + \underbrace{\mathbf{M}_{b,F}}_{=0}. \tag{12} $$

The gravity of the jth aircraft is defined in the Newtonian reference frame as

$$ \mathbf{W}_{n,j} = \begin{bmatrix} 0, & 0, & m_j\, g \end{bmatrix}^T \tag{13} $$

where m_j is the mass of the jth aircraft and g is the gravitational acceleration. The thrust of the jth aircraft is calculated with

$$ \mathbf{T}_{b,j} = \begin{bmatrix} F_j, & 0, & 0 \end{bmatrix}^T \tag{14} $$

where F_j is the thrust of the jth engine.

Aerodynamic forces and moments are generated by the wing, horizontal stabilizer and vertical stabilizer. The overall wing is built up by the wings of the single aircraft. As a consequence, a wing with a high aspect ratio is formed. The aerodynamic forces and moments are calculated in MATLAB with the vortex lattice method described in [6]. For this purpose, the wing is divided into a finite number of surfaces. The flow conditions on every surface depend on both the air density and aerodynamic parameter (angle of attack, sideslip angle and airspeed) that are also a function of the yaw rate of the whole formation and the pitch and roll rate of every aircraft. The software tool Autolev / Motion Genesis computes those kinematic equations after the definition of motion constraints. Based on the aerodynamic conditions, the vortex

[2] In flight mechanics often called geodetic reference frame that is considered as an inertial system.

lattice method determines lift, yaw (considering also the zero drag coefficient) and induced drag of every surface. By rotation of the normal vectors of the surfaces, flap deflections are considered. For the MBA every single aircraft is equipped with flaps along the complete left $\eta_{K,left}$ and right wing $\eta_{K,right}$ with 25% flap chord. Based on the aerodynamic forces at every surface and the corresponding collocation point, lift, induced drag and yaw can be assembled to each single aircraft. If the surface collocation point of the complete wing belongs to the ith aircraft, the forces are assigned to the ith aircraft. The corresponding aerodynamic moments are calculated by the lever arm of the surface collocation point (that belongs to the ith aircraft) to the center of gravity of the ith aircraft. To consider the downwash, horizontal and vertical stabilizer are included to the vortex lattice computation. The forces and moments can be directly assigned to the corresponding aircraft. The influence of rudder ζ and elevator η with 25% flap chord of vertical and horizontal stabilizer is computed by rotation of the normal vector of the corresponding surfaces. Finally, the part of the zero drag is added to each aircraft.

2.3 Linear Analysis of the Multi-body Aircraft

Based on the equation of motion, a Simulink Model is generated and linearized to analyze the flight dynamics of the formation. Additionally to the previous introduced flight dynamic model, the difference of the yaw to the yaw angle of the main aircraft

$$\Delta\Psi_i = \Psi_5 - \Psi_i \quad \text{with} \quad i \in \{1, \ldots, 10\} \setminus \{5\} \tag{15}$$

is considered as state instead of the absolute yaw angle of every aircraft. The state vector

$$\mathbf{x} = \begin{bmatrix} q_{\mathrm{AC5}}, \alpha_{\mathrm{AC5}}, V_{\mathrm{AC5}}, \gamma_{\mathrm{AC5}}, r_{\mathrm{AC5}}, \beta_{\mathrm{AC5}}, \ldots \\ p_{\mathrm{AC5}}, \Phi_{\mathrm{AC5}}, \mathbf{x}_{\mathrm{AC1}}, \mathbf{x}_{\mathrm{AC2}}, \mathbf{x}_{\mathrm{AC3}}, \mathbf{x}_{\mathrm{AC4}}, \cdots \\ \mathbf{x}_{\mathrm{AC6}}, \mathbf{x}_{\mathrm{AC7}}, \mathbf{x}_{\mathrm{AC8}}, \mathbf{x}_{\mathrm{AC9}}, \mathbf{x}_{\mathrm{AC10}} \end{bmatrix}^T \quad \text{with} \quad \mathbf{x}_{\mathrm{AC}i} = \begin{bmatrix} q_{\mathrm{AC}i} \\ \Theta_{\mathrm{AC}i} \\ p_{\mathrm{AC}i} \\ \Phi_{\mathrm{AC}i} \\ \Delta\Psi_{\mathrm{AC}i} \end{bmatrix}^T \tag{16}$$

has 53 elements (resulting of generalized speeds and coordinates). The fifth aircraft is selected as the main aircraft. A first analysis showed that the eigenvalues related to the yaw motion of every aircraft are close to the origin of the complex plane. Hence those nine states are neglected and the state vector is reduced to 44 elements. The eigenvalues of the system are plotted in Fig. 2. Twelve out of these eigenvalues are unstable. In total, the system has eight real eigenvalues (two are unstable) and 18 complex conjugate eigenvalue pairs (five are unstable). Based on the eigenvectors, a clear separation between lateral, longitudinal and linkage eigenvalues is not possible. The eigenvectors shows a strong coupling between all states in all modes.

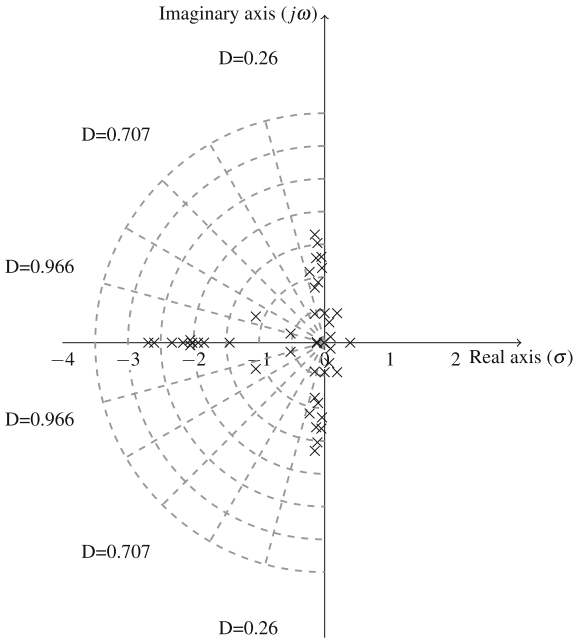

Fig. 2 Illustration of the eigenvalues of the linearized Multi-body HALE Aircraft in the complex plane

Nevertheless, a short period mode, a phygoid, a Dutch roll, an unstable spiral as well as roll and pitch linkage modes are recognizable. In [8] the eigenvectors for a formation of three coupled aircraft are investigated in detail.

3 Control Law Design

Although the aircraft dynamics strongly deviate from classical aircraft, the cascade control principle for conventional aircraft is applied to the Multi-Body aircraft. Hence, the flight path control laws contain three loops: The basic flight control law shall ensure damping of rates, airspeed, and wing shape holding control, while the outer-loop is used for attitude control (flight control) and flight path control (flight guidance). Only cruise flight is considered. The HALE aircraft shall operate in the mission altitude without significant altitude change, but with heading changes to ensure a cruise flight above a certain area. Therefore basic control laws are required to control pitch as well as bank angle of the aircraft. Attitude control is achieved with a special concept. The left middle aircraft is used as reference for the pitch angle of all left aircraft and the right middle aircraft for the other ones. In a left side turn, the left aircraft reduce their pitch angle, while the other aircraft hold or increase the pitch. With this, an imbalance in the lift distribution occurs and the aircraft banks to the left side. This is nothing else than the classical aileron concept. If the pitch

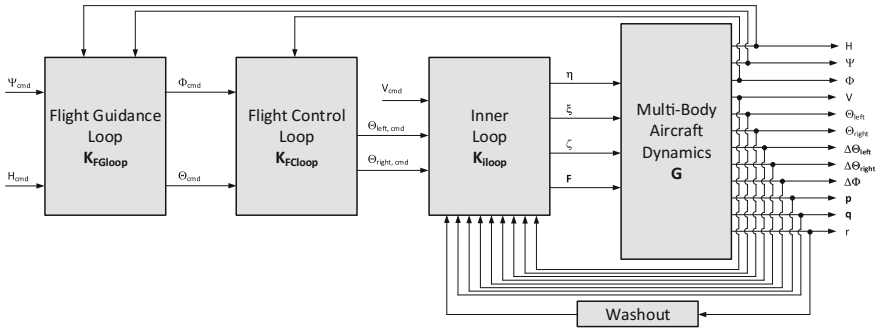

Fig. 3 Block diagram for the cascade flight path control law structure of the MBA

angle of the formation is changed, the demand values of left and right pitch angle have to be identical. Left and right pitch angle are controlled within the inner-loop. Changing of the demand values for left and right pitch angle for attitude control is carried out in the first outer-loop. Based on the attitude control, the second outer-loop for azimuth and altitude control is designed. Figure 3 illustrates the corresponding control law structure. The outputs $\Delta\Theta$ and $\Delta\Phi$ represent the wing shape differences and will be introduced in Sect. 3.2. In addition the inner-loop and two outer-loops, a washout filter is included in the flight control system. Because of the yaw damping, the inner-loop tries to damp also steady yaw rates that occur in turned flight. This is not desirable. With the help of a washout only frequencies relating to the Dutch roll are passed to the inner-loop. Steady yaw rates are not affected.

3.1 Requirements

Requirements for the flight control laws are derived from the analysis of the nominal plant and the aircraft design. The nominal plant has ten unstable eigenvalues. The stabilization of the plant is the main requirement of the flight control law. After the Helios mishap, the NASA in its function as an investigation organization recommend the use of nonlinear methods in the aircraft modeling and the flight control law design [12]. Multi-Body aircraft's equations of motions are nonlinear due to the trigonometric functions caused by joint modeling and kinematic differential equations of the individual aircraft. The flight control law design process shall consider those nonlinear effects. Due to gusts and turbulence, disturbances act on the aircraft that have to be rejected by damping of the rates [2] and by an airspeed controller. Flying over a one-year period with solar energy requires a low energy consumption that is ensured by flying with minimum power consumption, which, in turn, requires flying at a high lift coefficient. The aircraft operates close to the stall speed. To avoid stall, the flight control law has to achieve speed holding with high precision. In a basic investigation it turned out that the planar wing is optimal for low induced drag.

This leads to the requirement that the wing shape has to hold straight. To save energy, an extensive control surface activity has to be avoided. The long wing carries the danger of stall in turned flight. The outer wing has a high airspeed while the inner wing airspeed is very low.

Regarding airspeed and bank angle control, quantitative requirements can be defined. The aircraft flies with 90% of the maximum lift coefficient. To avoid stall, a maximum drop in the airspeed of 1.198 $\frac{\mathrm{m}}{\mathrm{s}}$ is allowed. This maximum airspeed reduction has to be considered also in turn flight. While the aircraft yaws, the airspeed is increased on the outside of the curve and decrease on the inside of the curve. Considering the half span of the aircraft and the maximum permissible airspeed drop, the maximum yaw rate is $0.64^\circ\ \mathrm{s}^{-1}$. An alternative approach would include the direct control of the local angles of attack instead of controling the speed of the (central) reference aircraft of the flight formation. Because such an approach would require more sensors and thus render the Flight Control Law more complex, it is not yet taken into account. Note, however, that measuring the local angles of attack is actually conceivable for the real application case of a HALE aircraft, eventually allowing to achieve a flight envelope protection.

Quantitative requirements for the flight path flight control law, like described in SAE AS94900 for piloted aircraft, do not exist for unmanned aircraft (especially for HALE). Those requirements depend on the actual mission. Currently, the MBA HALE shall be used for surveillance task and broadcast of television or internet. The altitude of the aircraft shall be maintained and heading changes shall be carried out in an adequate time and with an adequate radius above the area of interest. In this basic investigation only the functionality of a flight path with an MBA is shown.

3.2 Inner-Loop Control Law

The flight dynamics of the MBA are described as a nonlinear multiple input, multiple output (MIMO) differential equation system with significant coupling between the state variables. In general, there exist a variety of control design methods for nonlinear plants. In this paper the $\mathcal{H}_\infty$ robust control design method is used to describe the nonlinear dynamics as uncertainties. This method allows a definition of the requirements in the frequency domain and can deal directly with an uncertainty description during the design process [15]. A disadvantage of the method is the high order of the control laws. Nevertheless the computation effort can be distributed to all ten flight control computer.

The inner-loop shall achieve stability, damp pitch (every aircraft), roll (every aircraft) and yaw (formation) rate and controls the left and right pitch angle as well as the airspeed. The differences in the pitch angles are expressed by

$$\begin{aligned} \Delta\Theta_i &= \Theta_{\mathrm{AC5}} - \Theta_{\mathrm{AC}i} \quad \text{with} \quad i \in \{1, \ldots, 4\}, \\ \Delta\Theta_i &= \Theta_{\mathrm{AC6}} - \Theta_{\mathrm{AC}i} \quad \text{with} \quad i \in \{7, \ldots, 10\}, \end{aligned} \tag{17}$$

with the fifth aircraft (Θ_{AC5}) and sixth aircraft (Θ_{AC6}) as reference for left and right side pitch angle. The bank angle differences are formulated by deviation of the separate aircraft to the fifth aircraft (as reference aircraft) with

$$\Delta\Phi_i = \Phi_{\mathrm{AC5}} - \Phi_{\mathrm{AC}i} \quad \text{with} \quad i \in \{1, \ldots, 10\} \setminus \{5\}. \tag{18}$$

Those 17 differences lead to 41 total output values (21 rates, 17 wing shape differences, left and right pitch angle, and the airspeed) that are controlled within the inner-loop. As input variables all elevator deflections are used. The left and right wing flap are summarized into a common aileron

$$\xi_{\mathrm{AC}i} = \eta_{\mathrm{K,\,right,\,AC}i} - \eta_{\mathrm{K,\,left,\,AC}i} \quad \text{with} \quad i \in [1, \ldots, 10] \tag{19}$$

of every aircraft. The thrust and the rudder are set to identical values for every aircraft. This leads to 21 input variables. Hence, the linearized state-space model used for the inner-loop design is

$$\begin{aligned} \dot{\mathbf{x}}(t) &= \mathbf{A}\mathbf{x}(t) + \mathbf{B}\mathbf{u}(t)\ , \\ \mathbf{y}(t) &= \mathbf{C}\mathbf{x} + \mathbf{D}\mathbf{u}(t) \end{aligned} \tag{20}$$

with $\mathbf{y}$ as control variables, $\mathbf{u}$ as control inputs and $\mathbf{x}$ as states. By applying the Laplace transformation (assuming that the feedforward matrix $\mathbf{D}$ is equal to zero), this state-space models yields the system

$$\begin{aligned} s\,\hat{\mathbf{x}}(s) &= \mathbf{A}\hat{\mathbf{x}}(s) + \mathbf{B}\hat{\mathbf{u}}(s)\ , \\ \hat{\mathbf{y}}(s) &= \mathbf{C}\hat{\mathbf{x}}(s) \end{aligned} \tag{21}$$

that describes the plant in the frequency domain. Hence, the transfer function of the plant for inner-loop design is determined by

$$\mathbf{G}(s) = \hat{\mathbf{y}}(s)\ \hat{\mathbf{u}}^{-1}(s) = \mathbf{C}\left[s\,\mathbf{I} - \mathbf{A}\right]^{-1}\mathbf{B}. \tag{22}$$

3.2.1 $\mathcal{H}_\infty$ loop shaping

Figure 4 illustrates the augmented plant that is used for the $\mathcal{H}_\infty$ synthesis. The subject of the applied loop shaping is to minimize γ of the norm

$$\left\|\mathbf{F}_l(\mathbf{P}, \mathbf{K})\right\|_\infty < \gamma \tag{23}$$

under the constraint that $\mathbf{K}$ stabilizes the plant. The lower linear fractional transformation $\mathbf{F}_l$ represents the closed loop transfer function from the exogenous inputs to the exogenous outputs. The exogenous inputs are the demand values $\mathbf{r}$ for output values $\mathbf{y}$ that are controlled within the inner and disturbances values $\mathbf{d}$ that represent wind velocities acting on every aircraft. As discussed later, the output of the uncer-

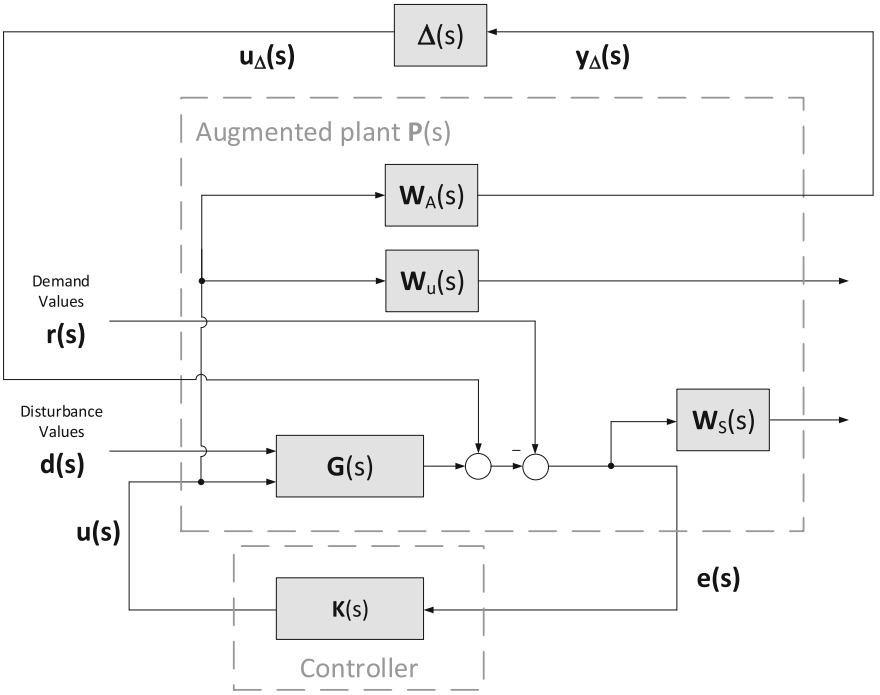

Fig. 4 Block Diagram of the $\mathcal{H}_\infty$ inner-loop synthesis with design weights $\mathbf{W}_S$, $\mathbf{W}_U$, deviation matrix $\mathbf{W}_A$ for an additive perturbation configuration and uncertainty matrix Δ

tainty matrix $\mathbf{u}_\Delta$ are also used as inputs in the control law design. The exogenous outputs are the weighted control inputs $\mathbf{W}_u\mathbf{u}$ to restrict controls, and the weighted error of the control values $\mathbf{W}_e\mathbf{e}$ to shape the sensitivity functions. Using an additive input perturbation configuration to describe the uncertainties, the deviation matrix $\mathbf{W}_A\mathbf{u}$ is used as additional exogenous output. For the use of normalized weights, the plant has to be normalized to the maximum input signal $u_{\max,i}$, the maximum disturbance values $d_{\max,j}$ and the maximum errors $e_{\max,k}$ [15]. The general input vector

$$\tilde{\mathbf{u}} = [\mathbf{u} \quad \mathbf{d}]^T \tag{24}$$

collects the control inputs and disturbance values. The maximum values for every general input $l \in \{1, \ldots, i+j\}$ and every output k are collected in two diagonal matrices with

$$\mathbf{D}_{\tilde{u}} = \operatorname{diag}\left(\tilde{u}_{\max,l}\right) \quad \text{and} \quad \mathbf{D}_e = \operatorname{diag}\left(y_{\max,j}\right). \tag{25}$$

In the case of the flight control law for the MBA, the maximum input signal for the elevator, ailerons and rudder is set to 10° and for the thrust to 50 N. According to

Table 2 Parameter of the sensitivity weight for the different control variables

	Number	Bandwidth	Target error	Target overshoot
		$\omega_{\mathrm{BW}}\ \left[\mathrm{rad\ s^{-1}}\right]$	A	M
Pitch rate	10	10	100	1.15
Roll rate	10	10	100	1.15
Yaw rate	1	10	100	1.15
Bank angle differences	9	10	100	1.15
Left pitch angle differences	4	10	100	1.15
Right angle differences	4	10	100	1.15
Left pitch angle	1	5	100	1.1
Right pitch angle	1	5	100	1.1
Airspeed	1	5	100	1.1

the certification specification for large aircraft CS-25 the maximum gust velocity is 6.36 $\frac{\mathrm{m}}{\mathrm{s}}$.[3] This value is rounded to 7 $\frac{\mathrm{m}}{\mathrm{s}}$ and used as maximum disturbance value. The error for the pitch and roll rates is set to 5 $\frac{1^\circ}{\mathrm{s}}$. The maximum error for the yaw rate follows from the requirements with 0.64 $\frac{1^\circ}{\mathrm{s}}$. The error of wing shape differences is set to 5° and for left and right pitch angle to 5°. Based on the predefined requirements, a maximum airspeed error of 1.198 $\frac{\mathrm{m}}{\mathrm{s}}$ is considered. The normalized plant $\mathbf{G}_n$ is computed with

$$\mathbf{G}_n = \mathbf{D}_e^{-1}\,\mathbf{G}\,\mathbf{D}_u\,. \tag{26}$$

The performance weights for shaping the sensitivity function are defined as block-diagonal matrix with the transfer function

$$w_{\mathrm{S}} = \frac{\frac{s}{M} + \omega_{\mathrm{BW}}}{s + \omega_{\mathrm{BW}}\ A}, \tag{27}$$

on the main diagonal. The parameter for the different control variables are listed in Table 2. The weight for the control surface deflections is selected with the transfer function

$$W_{\mathrm{U}} = \mathrm{diag}\left(\frac{\left(\frac{1}{\omega_{\mathrm{BW,\,actuator}}}s + 1\right)^2}{10\left(\frac{1}{10\omega_{\mathrm{BW,\,actuator}}}s + 1\right)^2}\right) \tag{28}$$

[3]The MBA belongs to CS-23 aircraft, but the flight envelope in terms of gust ends at 15,240 m (CS 23.333, [3]). Since the CS-25 considers altitudes up to 18,288 m (CS 25.341, [4]), this specification is applied.

that shall ensure that the controller only commands inputs that are within the bandwidth of the actuators $\omega_{\text{BW, actuator}} = 18.95\ \frac{\text{rad}}{\text{s}}$. The uncertainty is described as unstructured uncertainty in the additive perturbation configuration with

$$\mathbf{W}_{\text{A}}(s)\,\Delta(s) = \mathbf{G}_{\text{P},i} - \mathbf{G}_0,, \tag{29}$$

with $\mathbf{G}_0$ as nominal system (based on the linearization) and $\mathbf{G}_{\text{P},i}$ as family of perturbed system dynamic that cover the nonlinearities. The determination of the perturbed systems is carried out as follow: The considered linear plant arises out of the linearization of the nonlinear equation of motion. Linearization accuracy drops off for highly nonlinear systems since the applied Taylor series truncates quadratic and higher order terms of the derivation variables [1]. Hence, the linear approximation of the fully nonlinear trajectory is only valid in a small interval around $\delta x = 0$. To increase the range of valid solutions to an interval of interest $[\delta x_1, \delta x_2]$, the gradient of the fully nonlinear trajectory of every δx within the range of interest is determined. Based on the maximum $\left(\frac{\partial f}{\partial x}\right)_{\max}$ and minimum gradient $\left(\frac{\partial f}{\partial x}\right)_{\min}$, the maximum negative and positive variation to the nominal parameter $\left.\frac{\partial f}{\partial x}\right|_{\substack{x=x_0\\u=u_0}}$ is determined. Those variations represent the possible range of the corresponding entry in the system matrix $\mathbf{A}$ and, hence, the parameter can be assumed as uncertain. It has to be noted that the parameter could be varied only negatively or positively to the nominal parameter. The same procedure can be carried out for the input values. The differences between fully nonlinear trajectory and linear approximation for one entry of the system matrix and input matrix are exemplary illustrated in Fig. 5. The consideration of all parameter

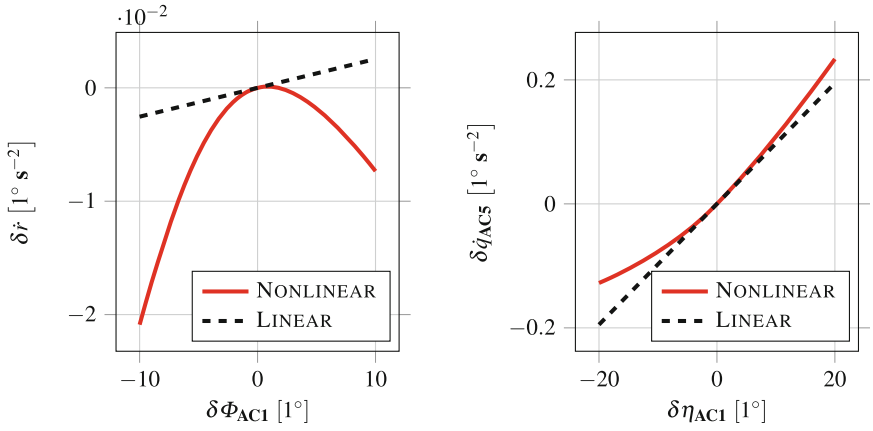

(a) Effect of changes in the bank angle of the first aircraft on the yaw rate derivative of the formation

(b) Effect of changes in the elevator of the first aircraft on the pitch rate derivative of the fifth aircraft

Fig. 5 Differences between the fully nonlinear trajectory and the linear approximation

would lead to a very large computation effort. In order to avoid this, conditions are introduced to decide if a parameter is assumed as uncertain or not. If the difference between calculated maximum or minimum slope in the range of interest and the slope in system or input matrix is smaller than 0.1, the parameter is not assumed to be uncertain. After applying this criteria, the system matrix contains 245 uncertain parameter that correspond to 12% of all entries. In the input matrix, 476 uncertain parameter remain, corresponding to 22% of all derivatives of the input matrix. In sum, 721 uncertain parameter are identified for the whole system description. Since the plant is not squared (different numbers of inputs and outputs), the unstructured uncertainties have to describe by a reduced number of inputs and outputs. Most uncertainties in the system matrix are related to the rates and the uncertain parameter in the input matrix are exclusively connected to the aerodynamic surface deflections. Hence, only the 21 rates (pitch and roll rate of every aircraft and the yaw rate of the formation) and the 21 aerodynamic control surface inputs (aileron and rudder of every aircraft as well as the rudder that is equal for all aircraft). The plant is now squared. With the help of MATLAB the uncertain plant is determined and a sample of 7210 random uncertain models is generated. Different unstructured uncertainty descriptions are applied to the uncertain models and the plant, since the results differs from method to method [15]. The criteria of low entries in the deviation matrix is fulfilled by using an additive perturbation configuration. The maximum singular values for the differences of all 7210 uncertain models to the nominal plant together with an upper bound are determined with the transfer function

$$w_{\mathrm{a}} = \frac{\frac{1}{0.05}s}{\left(\frac{1}{0.05}s+1\right)\left(\frac{1}{1}s+1\right)}. \tag{30}$$

The weight and 50 randomly selected maximum singular values of the differences between uncertain models and the nominal plant are illustrated in Fig. 6. The results of the random sampling are representative for the complete uncertain model family.

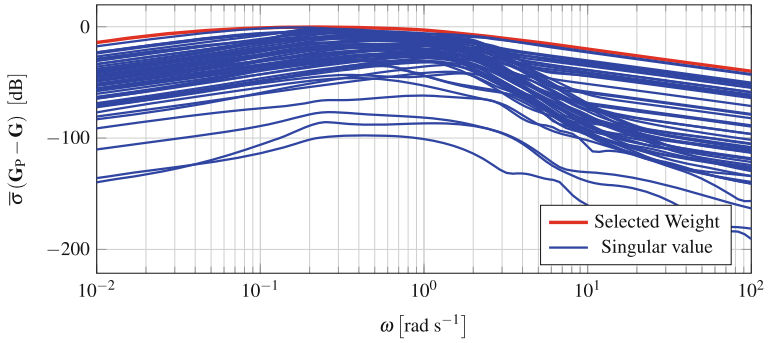

Fig. 6 Maximum singular value of the differences between 50 randomly selected uncertain models and the nominal plant and the corresponding weight for the deviation matrix

The deviation matrix $\mathbf{W}_A$ is a block diagonal matrix with the transfer function of Eq. 30 on the main diagonal.

With the introduced weights, the control law process is carried out and a control law with the order of 191 is calculated. The controller itself is stable and the maximum frequency is 7.2 Hz. Evaluation of robust stability is carried out by using the $\mathbf{M}\Delta$ structure. In this control loop description, the controller and augmented plant are connected with each other. This leads to the system $\mathbf{M}$. As exogenous inputs and outputs for this system only the outputs of the uncertainty matrix Δ and outputs of the deviation weight are used. Based on the small gain theorem, the condition

$$\overline{\sigma}(\mathbf{M}) < 1 \tag{31}$$

has to be fulfilled for robust stability with $\overline{\sigma}$ as maximum singular value [15]. The developed control law fulfills the condition of Eq. 31 is robustly stable against the modeled uncertainties. Since the order is too high, model reduction with the balanced truncation method is applied [15]. To define the minimal achievable control law order, the order of the control law was reduced from full (order 191) to one by one order steps until the stop criteria (that robust stability is still achieved) is violated. In this context, the control law was successfully reduced to the order of 61.

3.2.2 Results

The designed inner-loop controller with an order of 61 is now evaluated with respect to the time dimension. Therefore, the control law is implemented in the non-linear simulation environment of the MBA. In a nonlinear simulation study, the left and right pitch angle command is increased to 5°. The results are illustrated in Fig. 7. All pitch angles respond simultaneously. This indicates that the wing shape controller relating to the pitch angle works well. A steady error occurs, which is expected by considering the sensitivity function. The steady value of the pitch angle is reached within 20 s. The corresponding elevator deflections are low. No high frequency deflections are identified. Deviations in the bank angle are very low and, hence, the requirements of the wing shape holding relating to the bank angle is completely fulfilled. Also, the amounts and frequencies of wing flap deflections are low and within an acceptable limit. The drop in the airspeed is very low. That was one requirement to avoid stall conditions. Nevertheless, the thrust is very high and exceeds the limits of the engine that works in steady flight condition with half power. Thus, for the outer-loops it has to be considered to limit the maximum pitch angle to 2°. In summary, the inner-loop fulfills all requirements completely.

The aircraft response to a non-uniform distributed vertical gust is investigated. Figure 8 shows the nonlinear results. The gust acts at the second aircraft and is modeled as an $1 - \cos$ gust with

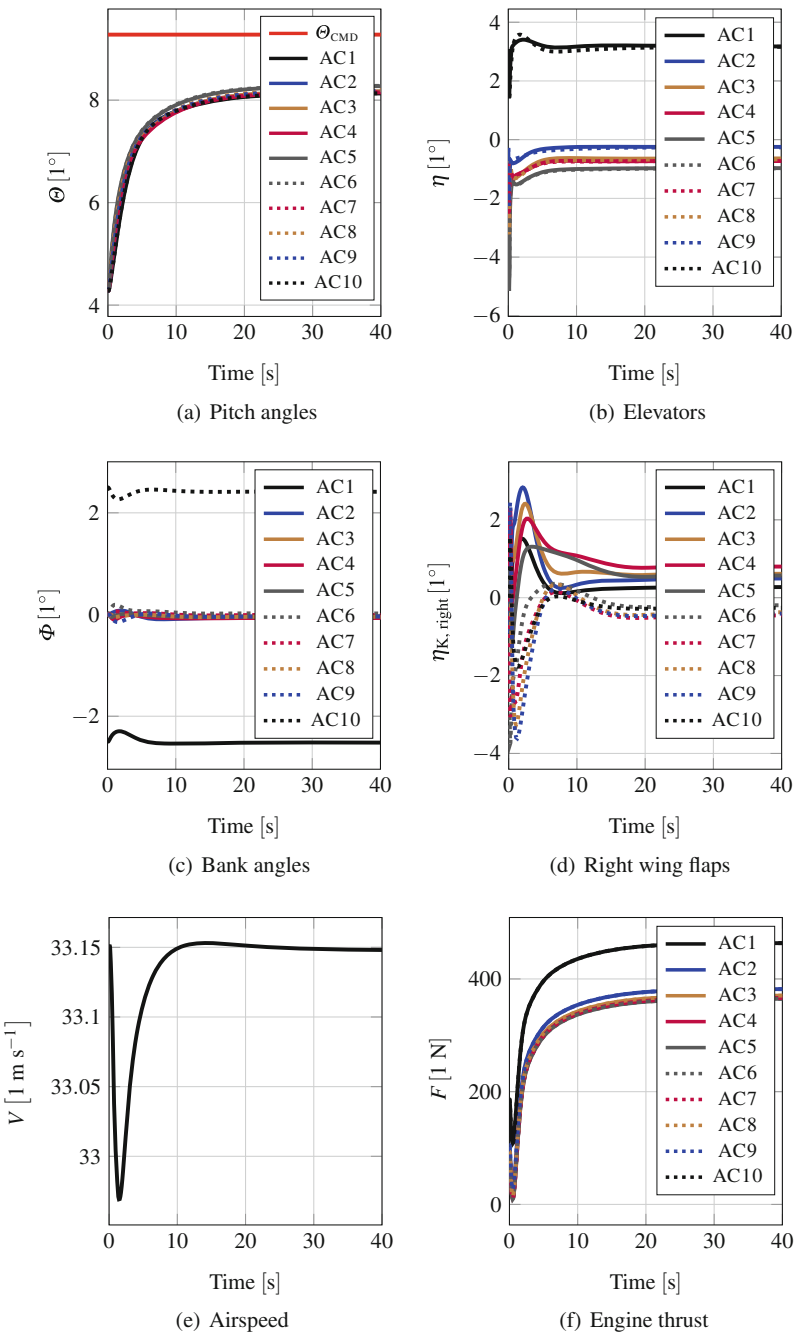

(a) Pitch angles (b) Elevators

(c) Bank angles (d) Right wing flaps

(e) Airspeed (f) Engine thrust

Fig. 7 Nonlinear simulation results of inner-loop for a step input to the *left* and *right side* pitch angle command of 5°

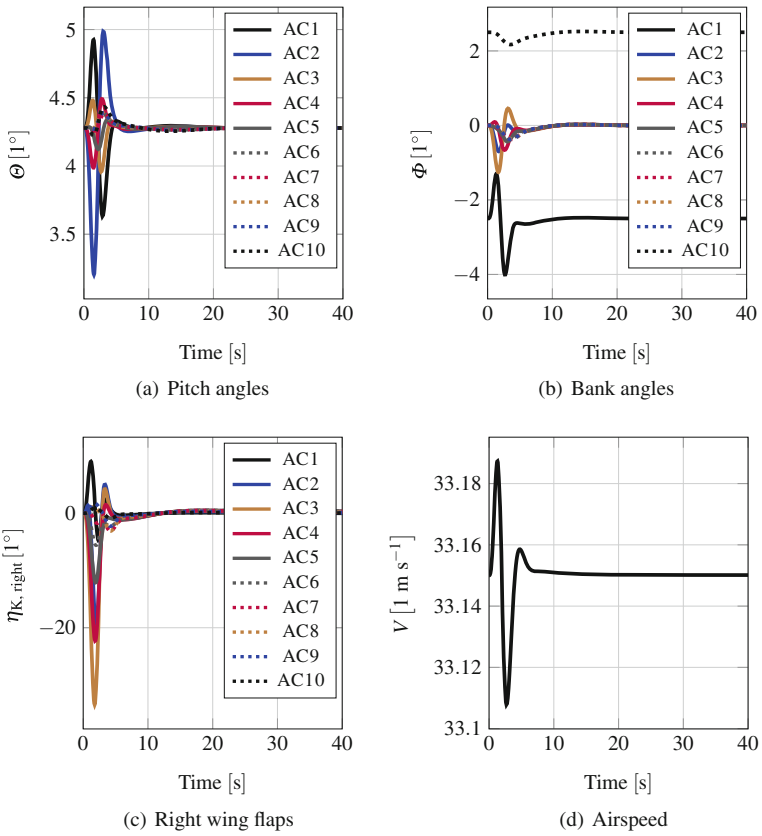

(a) Pitch angles (b) Bank angles

(c) Right wing flaps (d) Airspeed

Fig. 8 Nonlinear simulation results of inner-loop for a vertical gust acting on the second aircraft

$$w_w(t) = \frac{U_{\text{gust}}}{2}\left(1 - \cos\left(2\,\pi\,\frac{V_{\text{ref}}}{2}\,t\right)\right), \tag{32}$$

with $U_{\text{gust}} = 6.36\ \frac{\text{m}}{\text{s}}$ as gust amplitude (c.f. CS-25 for an altitude of 18,288 m [4], L as gust length that is equal to 25 times the chord length and $V_{\text{ref}} = 33.15\ \frac{\text{m}}{\text{s}}$ as reference airspeed [18]. In the aircraft response, it becomes clear that the gust acts at the second aircraft, because the bank of the first and third aircraft are contrarily affected. The values of the wing shape differences are small and acceptable. Also, the airspeed changes are within satisfactory limits, since the airspeed drop is very low. Although a non-uniformly distributed gust acts on the formation, the bank angle changes are very small. The linkages, as shown by the bank angle differences, do not transfer bending moments and hence the Multi-Body HALE aircraft is most suitable to reject non-uniformly distributed gust. The thrust changes are very low, but the wing flap deflection of the third aircraft is very high. Because of the low speed operation of the aircraft such a deflection should be acceptable.

In the nonlinear simulation, the results with respect to the shaped sensitivity function are confirmed. All controller work as required and fulfill the requirements. Wing shape holding is achieved in gust and maneuvers. The airspeed does not drop below the minimum value. Non-uniform distributed gusts are rejected by the inner-loop, which is a big advantage in comparison to state of the art HALE aircraft [17].

3.3 Outer-Loop Control Law

The outer-loop design is based on the single input, single output description between the input variable and the control variable. Since pitch angle control is already established by the inner-loop, the outer-loop relating to flight control has only to cover the functionality of bank angle control. For turned flight, at first a washout filter is integrated in the inner-loop. Therefore, a transfer function with

$$G_{\text{Washout}} = \frac{T_{\text{D}} s}{T_{\text{D}} s + 1} \tag{33}$$

is selected with $T_{\text{D}} = 0.2$ s. This value is based on the Dutch roll frequency with inner-loop. The integration of this filter destabilizes. This change is expected since the spiral mode has to be unstable for turned flight. The left $\Theta_{\text{left, cmd}}$ and right $\Theta_{\text{right, cmd}}$ pitch angle command to the inner-loops represent an overlay of the pitch angle command Θ_{cmd} and the signal caused by the bank angle controller ξ_{bank} with

$$\begin{aligned} \Theta_{\text{left, cmd}} &= \Theta_{\text{cmd}} + \xi_{\text{bank}} \\ \Theta_{\text{right, cmd}} &= \Theta_{\text{cmd}} - \xi_{\text{bank}} \end{aligned}. \tag{34}$$

The bank angle controller is designed with the root locus method [2]. The transfer function from ξ_{bank} to the bank angle is used. Therefore, the system is reduced by the balanced truncation to a second order system. The corresponding control law is

$$\xi_{\text{bank}} = k_{\xi\Phi} \left(\Phi_{\text{cmd}} - \Phi_{\text{AC5}} \right) \tag{35}$$

and the proportional gain is determined with $k_{\xi\Phi} = 2$. With this approach, pitch as well as bank angle are controlled for the MBA and the outer-loop relating to flight control is designed.

Regarding the flight control outer-loop, the pitch angle Θ_{cmd} and the bank angle Φ_{cmd} are available as input values and the altitude H and the azimuth Ψ have to be controlled by the flight guidance outer-loop. This classical flight control principle is also applied to conventional aircraft [2]. For both values, a proportional control law with

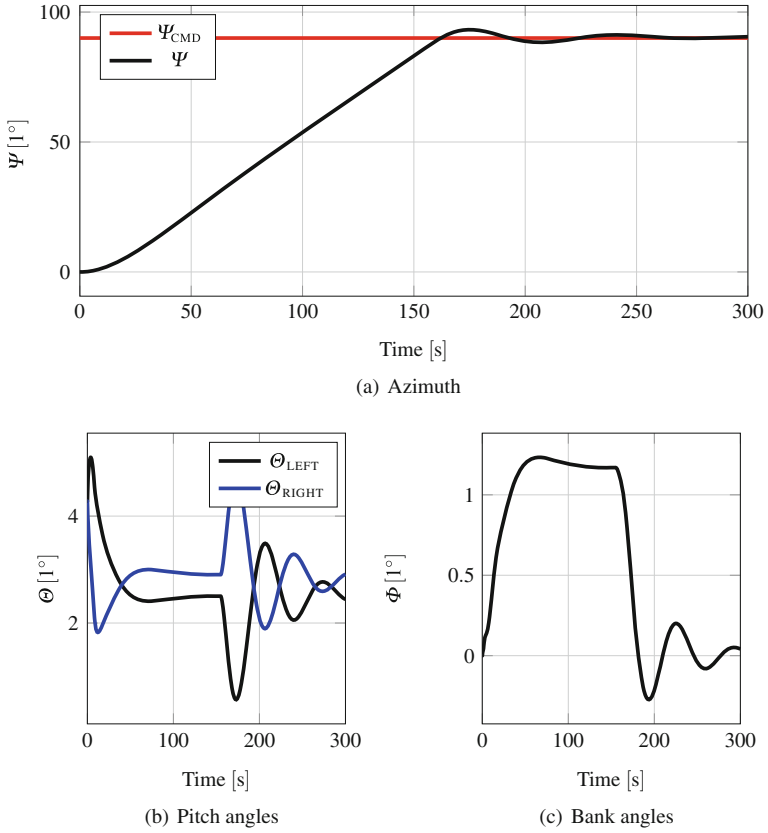

(a) Azimuth

(b) Pitch angles

(c) Bank angles

Fig. 9 Nonlinear simulation results of flight guidance outer-loop with a commanded azimuth of 90°

$$\begin{aligned} \Theta_{\text{cmd}} &= k_{\Theta H} \underbrace{(H_{\text{cmd}} - H)}_{e_H} \quad \text{and} \\ \Phi_{\text{cmd}} &= k_{\Phi \Psi} \underbrace{(\Psi_{\text{cmd}} - \Psi)}_{e_\Psi} \end{aligned} \tag{36}$$

is used. The maximum commanded pitch angle is limited to 2.0° for a lower required thrust. Having an altitude error of 5 m, the gain $k_{\Theta H}$ commands 2.0° to the flight control inner-loop. The bank angle command is bounded to 1° and $k_{\Phi \Psi} = 0.25$ is used for the azimuth control loop. The nonlinear simulation results for a step command in the azimuth angle of 95° are illustrated in Fig. 9. The MBA needs approximately 160 s until the demand value is reached. This corresponds to a yaw rate of 0.56° s^{-1}. A small overshoot occurs. The left and right side pitch angle react adversely to each other. In the intercept/capture phase of the desired azimuth, some low frequent and well damped oscillations occur. In summary, the proportional gain controller is able to achieve fast tracking of an azimuth.

4 Conclusion and Outlook

In this paper, a flight path flight control law for a Multi-Body HALE aircraft was presented. This aircraft is able to operate continuously one year in the mission altitude. Kane's formalism was used to assemble the equations of motion for the Multi-Body aircraft. The uncontrolled aircraft shows a nominal unstable behavior with 10 right hand side poles.

The developed flight control law bases on the classical cascade flight control principle. Since the flight dynamics of the MBA strongly differ to classical aircraft, a new design method and structure for the inner-loop had to be applied. Therefore, the H_∞ loop shaping in the frequency domain was successfully used. Besides a clear and unique definition of the requirements, the method allows the use of uncertainties to take non-modeled flight dynamics into account. With the design method, a robust inner-loop was designed that successfully stabilizes the plant and achieves wing shape holding, airspeed, left and right side pitch control as well as gust rejection. Especially the results of non-uniform distributed gust load rejection underline the benefit of a Multi-Body Hale aircraft in comparison to a one wing HALE aircraft. Based on the inner-loop flight control law, classical outer-loop flight control laws for azimuth angle and altitude control were applied. The formation follows the azimuth angle very fast. That allows surveillance and broadcast missions over a certain area.

Alongside the benefits of the design method for the inner-loop, the order of the designed inner-loop is very high (61). In the case of a classical aircraft, this order would be too high, but the Multi-Body aircraft concept offers new possibilities to handle the computational effort. Calculation routines can be distributed among many computers and this allows a fast computation even for high order control laws. A suitable concept has to be discussed in further investigations. The functionality of the control laws (especially for wing shape holding) shall be proven in a flight test campaign with a small Multi-Body aircraft demonstrator that is already constructed and possesses the same degrees of freedom like the HALE Multi-Body aircraft.

References

1. Armellin R et al (2010) Nonlinear mapping of uncertainties: a differential algebraic approach. In: 4th international conference on astrodynamics tools and techniques, ESAC, Spain
2. Brockhaus R, Alles W, Luckner R (2013) Flugregelung, vol 3. Springer, Berlin
3. European aviation safety agency, certification specifications and acceptable means of compliance for normal, utility, aerobatic, and commuter category aeroplanes (CS-23), amendment 4, 2015
4. European aviation safety agency, certification specifications and acceptable means of compliance for large aeroplanes (CS-25), Amendment 18, 2016
5. Gu DW, Petkov PH, Konstantinov MM (2005) Robust control design with MATLAB®. Springer Science & Business Media, Berlin
6. Katz J, Plotkin A (2001) Low-speed aerodynamics. Cambridge University Press, Cambridge
7. Kane, Thomas R, Levinson, David A, (1985) Dynamics, theory and applications. McGraw Hill, New York

8. Köthe A, Luckner R (2015) Flight mechanical modeling and analysis of Multi-Body aircraft. In: International forum on aeroelasticity and structural dynamics (IFASD). St. Petersburg, Russia
9. Lee B, Poomin P, Chuntaek K (2014) Power managements of a hybrid electric propulsion system powered by solar cells, fuel cells, and batteries for UAVs. In: Handbook of unmanned aerial vehicles. Springer, Berlin
10. Levinson, DA, Kane, TR (1990) AUTOLEV - a new approach to multibody dynamics. In: Multibody systems handbook. Springer, Berlin
11. Marsh G (2010) Best endurance under the sun. In: Renewable energy focus 11.5, Oxford
12. Noll TE et al (2004) Investigation of the Helios prototype aircraft mishap volume I mishap report. National aeronautics and space administration
13. Niewoehner RJ, Isaac IK (1994) Design of an autoland controller for a carrier-based F-14 aircraft using H_∞ output-feedback synthesis. In: American control conference, vol 3. IEEE, New York
14. Phillips WF (2004) Mechanics of flight. Wiley, New York
15. Skogestad S, Postlethwaite I (2007) Multivariable feedback control: analysis and design, vol 2. Wiley, New York
16. Tucker MR, Walker DJ (1997) H_∞ mixed sensitivity. In: Robust flight control. Springer, Berlin
17. Su W, Cesnik CE (2011) Dynamic response of highly flexible flying wings. AIAA J 49(2)
18. Wright JR, Cooper JE (2008) Introduction to aircraft aeroelasticity and loads. Wiley, United kingdom